JOURNAL OF MATERIALS SCIENCE **36** (2001) 451–460

Low temperature fracture properties of polymer-modified asphalts relationships with the morphology

L. CHAMPION, J.-F. GERARD*
Laboratoire des Matériaux Macromoléculaires, UMR CNRS 5627, INSA Lyon Bât. 403, 69621 Villeurbanne Cedex, France
E-mail: jfgerard@insa-lyon.fr

J.-P. PLANCHE, D. MARTIN
Centre de Recherche Elf de Solaize, Chemin du Canal - 69360 Solaize, France

D. ANDERSON
The Pennsylvania State University, University Park, PA 16801, USA

A methodology for studying the relationships between fracture behavior and morphology of polymer-modified asphalts used as binders was developed by using the linear elastic fracture mechanics (LEFM) method and confocal laser scanning and environmental and cryo-scanning electron microscopies. Different types of polymers were used as modifiers: (i) copolymers from ethylene and methyl acrylate (EMA), butyl acrylate (EBA) or, vinyl acetate (EVA); (ii) diblock or star-shape triblock styrene-butadiene copolymers (SB or SBS*). The 4 to 6 wt. % blends display an heterogeneous structure with a polymer-rich dispersed phase based on the initial polymer swollen by the aromatic fractions of the asphalt. The fracture toughness of the blends is higher than for the neat asphalt even if Klc of blends remains low compared to usual polymer blends due to the brittleness of the asphalt matrix. The fracture behavior which is strongly dependent on the nature of the polymer is discussed from the toughening mechanisms given for the filled polymers and the polymer blends. The EBA, SB, and SBS-based blends compared to the EMA and EVA-based ones display a higher Klc due to the elastomeric behavior of the polymer phase leading to a more efficient energy dissipation during crack propagation. The sample prepared with 4% crosslinked SB (Styrelf) and the corresponding physical blend (non-crosslinked) display the better fracture properties.

1. Introduction

Asphalt is a viscoelastic material at room temperature, i.e. it behaves as a viscous fluid at high temperature whereas it is a brittle solid at low temperature. One of the most promising methods for improving the asphalt performances at low temperature is by using additives such as polymers. Several types of polymers have been proposed and used as asphalt modifiers with additive contents as low as 3–6 wt. %, including elastomeric copolymers such as as styrene-butadiene rubbers, SBR [1], poly(styrene-b-butadiene), SB, and poly(styrene-b-butadiene-b-styrene), SBS [1–3]. The final volume fraction of the polymer-dispersed phase is higher that the initial one, about 20% by volume due to the swelling with the aromatic oily species of the original asphalt. The resulting blends, also called as physical blends, are generally unstable mixtures and macrophase separation can occur during long term storage times and/or at high temperatures. To overcome this demixing phenomenon, a dynamic vulcanization process can be done consisting in the *in-situ* crosslinking of the polymer dispersed phase [4]. In the United States, the Government passed legislation to add waste rubber like crumb rubber to their asphalt pavements [5, 6]. Others have modified asphalt with polyolefins such as polyethylene [3, 7, 8], ethylene vinyl acetate, EVA [8, 9], or EMA [10, 11]. The use of crumb rubber or recycled polyolefins is environmentally attractive because it offers alternative for recycling the plastics wastes.

The final properties of the asphalt-polymer blends depend on the morphology, i.e. the distribution of particle sizes and composition of the phases, but also on the interface between the asphalt continuous phase and the polymer-rich dispersed phase. From previous studies on styrene-butadiene block copolymer-modified asphalts [12], it was demonstrated that blends displays an emulsion-like morphology and the polymer is swollen by some fractions of the asphalt, mainly by the maltenes. As a consequence, the interfacial tension between the swollen polymer and the asphalt matrix

calculated from the Palierne' model is very low (about 10^{-5} N · m^{-1}). In addition, from the swelling of the polymer by the maltenes, the asphalt continuous phase is artificially enriched in asphaltenes by a "physical distillation" of the lighter species from the original asphalt, leading to a toughened matrix. Such an understanding of the physical modifications of both the polymer and the asphalt can be used to select the microstructure, i.e. the chemical nature, the molar mass, etc., of the polymer which is used as modifier.

In fact, as asphalt is brittle at low temperature, the thermal cracking of asphalt pavements is a serious problem in cold countries. Nevertheless, the current specifications do not specifically consider the failure mechanisms. Hesp [13–15] developed a method based on the linear fracture mechanics, LEFM, principles in order to characterize the fracture behavior of neat asphalts and polymer-modified asphalts at low temperatures. From his work, the fracture toughness of the polymer-modified asphalts at −20°C are higher than the toughness of the neat asphalt. Sabbagh and Lesser [16] also studied the mechanical behavior of polyolefin-modified asphalts using a three-point-bending beam method. For such materials, the low temperature fracture tests also showed an increase for KI_C with increasing the amount of polyethylene (from 0 to 5% by wt.).

The aim of this study was to establish relationships between the fracture properties, measured from the method developed by Hesp, and the morphology of polymer-modified asphalts. The effects of the chemical nature and the amount of polymer used for modifying the asphalt on the fracture toughness were also studied. For such a purpose, original methods were used to study the morphology of polymer-modified asphalts such as confocal laser scanning microscopy (CLSM). In addition, the environmental scanning electron microscopy (ESEM) and the cryo-scanning electron microscopy (CSEM) were used to examine the fracture surfaces in order to explain the differences in fracture properties for different modified binders.

2. Experimental

2.1. Materials

2.1.1. Asphalt

The neat asphalt used for the modified binders was a 70/100 penetration grade (penetration at 25°C: 85 1/10 mm; ring and ball softening point: 45.6°C) obtained from a Elf-Antar refinery and denoted G0078. The glass transition temperature of the asphalt is about –27°C and the crystallized fractions content is 5%. The generic composition based on the SARA (Saturates, Aromatics, Resins, Asphaltenes) fractions of the asphalt is given in Table I. The asphalt can be considered as a continuum and the SARA fractions are defined from the solubility in various solvents [17]. By definition, the asphaltenes precipitate in n-heptane whereas the maltenes are soluble in this solvent. Coupling thin layer liquid chromatography and flame ionization detection allows to distinguish maltene species by using successive solvents such as cyclohexane (saturates), dichloromethane (aromatics), and a dichloromethane/methanol/isopropanol mixture (70 : 25 : 5) (resins). The asphaltenes, having molar masses between about 800 and 3,500 g · mol^{-1} are formed of on numerous polycondensed aromatics and dangling aliphatic chains [18]. These species are associated to form graphitic stacks or micellar structures in solvents [18] which can be evidenced by small-angle X-Ray scattering (diameter about 2–4 nm). The saturates contain few linear alkanes which can be crystallized and have very low molar masses (about 600 g · mol^{-1}). The T_g of saturates is about −70°C and these ones display a dissolution/crystallization phenomenon between T_g and 100°C. The aromatics represent the largest fraction of the asphalt. These are based on less aliphatic chains with slightly condensed aromatic rings and display a T_g at about −20°C, i.e. close to that of the whole asphalt [19, 20]. The resins, also called naphteno-aromatics have a composition which is close to that of the asphatenes with a T_g at about 20°C.

The asphalt can be modeled as a colloidal suspension of asphaltenes peptized by the resins fractions [21, 22]. As a consequence, the structure changes as the temperature decreases from a newtonian fluid at high temperature (above 60°C) to a structure for which the peptization layers of resins are enough thick to reach percolation [12].

TABLE I Composition of the G0078 asphalt from the SARA fractions

Saturates fraction (%)	9.0
Aromatics fraction (%)	67.8
Resins fraction (%)	13.7
Asphaltenes (%)	9.4

2.1.2. Polymers used as modifiers

Two different types of copolymers, semi-crystalline and amorphous, were used for modifying the asphalts.

Semi-crystalline copolymers such as poly(ethylene-co-vinyl acetate), EVA, poly(ethylene-co-methyl acrylate), EMA, and poly(ethylene-co-butyl acrylate), EBA were supplied by ELF Atochem Company. The characteristics of the ethylene-based copolymers are reported in Table II. The weight fraction of the comonomer was determined by RMN ^{1}H. The rate of crystallinity was calculated from the measured melting enthalpy of the polyethylene-enriched phase in the copolymers and from the equilibrium melting enthalpy of a pure crystal of linear polyethylene (taken equal to 293 J·g^{-1} [23]).

The amorphous copolymer SB is a linear styrene-butadiene diblock copolymer whereas SBS_1^*, SBS_2^* and SBS_3^* are star-shape triblock styrene-butadiene copolymers. The weight fractions of the polystyrene and

TABLE II Physical properties of the semi-crystalline copolymers

Copolymer	Fraction of the comonomer (% wt)	T_g (°C)	Crystallinity rate (%)[(a)]
EVA-18	18.6	−22.2	25.7
EVA-28	28.4	−19.9	15.3
EMA-28	28.6	−26.4	9.4
EBA-35	33.9	−45.9	10.6

[(a)] After melting at 180°C for 5 minutes and cooling at room temperature (10 K · min^{-1}).

TABLE III Physical properties of the styrene-butadiene copolymers

Copolymer	Molar mass ($g \cdot mol^{-1}$)	Fraction of the polystyrene (% wt.)	T_g PB block/ PS block (°C)
SBS_1^*	240,000	41.1	−90.5/51
SBS_2^*	135,000	40.6	−89.6/62
S 1110		22.7	−100/66
SBS_3^*		29.8	−88/66

polybutadiene blocks and the molar masses were determined by RMN ^{1}H and size exclusion chromatography, SEC (Table III).

2.2. Processing of the polymer-modified asphalts

The asphalt modification was produced by mixing the asphalt and 4 to 6 weight % polymer under moderate shear rate (300 rpm) at 180°C for few hours. The mixture was poured in silicone molds at 180°C having the shape of the specimens for fracture tests and the samples were cooled down to room temperature at a cooling rate of 2 $K \cdot min^{-1}$.

As the morphologies of the blends were examined using confocal laser scanning microscopy (CLSM), 0.1% of a fluorescent probe (Rhodamin-B C.I. from Aldrich) was added to the semi-crystalline polymers to stain the copolymers and increase the contrast. As a consequence, the polymer-rich dispersed phase could be observed in the asphalt-rich phase. The copolymer and the Rhodamin-B were mixed in toluene at 70–80°C. Then, the solvent was removed at room temperature for one week. Differential scanning calorimetry was performed in order to ensure that the toluene was completely removed from the polymer. The stained polymer was then added to the asphalt in the same way as described previously. The blends with stained polymers were stored at −4°C for one week before observation to prevent the diffusion of the Rhodamin-B from the polymer-rich phase to the asphalt-rich phase.

2.3. Mode-I fracture test

The fracture test was carried out by using a three point bending beam method based on the ASTM E399-83 procedure. Samples with a V-shape pre-notch (angle 90°) were prepared using the method developed by Hesp [13–15]. As mentioned previously, the binder to be studied was reheated at 180°C and poured in a silicone mold ($25 \times 12.5 \times 175$ mm^3) having a 90° notch in its centre. The samples were stored at −20°C for 2 hours, removed from the mold, and kept for 18 hours at the test temperature, i.e. −20°C. The pre-notch was sharpened with a razor blade immediately before the test and the new crack length, denoted a, was measured under an optical microscope. The beams were placed in the environmental chamber for 10 minutes before mechanical testing. The crosshead speed was 0.6 $mm \cdot min^{-1}$ and the sample was loaded until the fracture crack propagated. The critical stress intensity factor, KI_C, was calculated according to the following equation [24] from tests conducted on 8 samples.

$$KI_c = \frac{P_f S}{BW^{3/2}} \times \frac{3\left(\frac{a}{W}\right)^{1/2}\left[1{,}99 - \frac{a}{W}\left(1 - \frac{a}{W}\right) \times \left(2{,}15 - 3{,}93\frac{a}{W} + 2{,}7\frac{a^2}{W^2}\right)\right]}{2\left(1 + 2\frac{a}{W}\right)\left(1 - \frac{a}{W}\right)^{3/2}}$$

where P_f is the failure load and S the span fixed to 100 mm. B and W are the sample depth (12.5 mm) and the specimen width (25 mm), respectively. The crack length, a, was measured for each sample.

2.4. Analyses of the morphologies

An environmental scanning electron microscope *(Electroscan Explorer 2010)* and a cryo-scanning electron microscope (Philips XL40 FEG-SEM) were used to examine the fracture surfaces. ESEM allows the examination of surfaces of practically any specimen, wet or dry, insulating or conducting, by allowing the presence of a gas in the specimen chamber [25, 26] but the resolution is limited.

The observation of asphalts with a conventional SEM is difficult because of the high vacuum requirements and their low T_g. The cryo-preparation and observation equipments for conventional SEM has been available for over two decades and applied to biomedical and materials specimens [27]. This innovation allows SEM observation of soft or liquid specimens at low-to-medium magnification. The fractured samples are coated with 4 nm of platinum at −165°C and transferred to the microscope.

The fractured specimens were stored for one to three days at −25°C before ESEM and CSEM experiments. The morphology was analyzed from the fracture surfaces of the specimens observed at respectively −5°C and −165°C by ESEM and CSEM.

Another way to analyze the morphology of the blends was to use the confocal laser scanning microscopy (CLSM). Samples from each type of the polymer-modified asphalts were prepared by squeezing the polymer-asphalt mixture between glass plates (100 μm-thick specimens). A Carl Zeiss laser scan microscope was used and the images were recorded in transmission mode using the He-Ne laser (543 nm wavelength) or the Ar laser (488 and 514 nm wavelengths). CLSM is a relatively new technique which can be used also to obtain 3-D images and has already been applied to the observation of several types of materials such as polymer blends [28], fiber-based polymer composites [29], or porous silicon [30].

3. Results and discussion

3.1. Morphology of the polymer-modified asphalts

The confocal laser scanning microscopy allows to observe the morphology of the polymer-asphalt blends by capturing the contrast between the two phases (Fig. 1). As reported previously, whatever the polymer type, the volume fraction of the polymer-rich phase in the polymer-asphalt blends is very high compared to the initial amount of polymer added to the asphalt [31]. The high volume fraction, which cannot be determined precisely from the CLSM micrographs, is explained by the swelling of the polymer by some fractions of

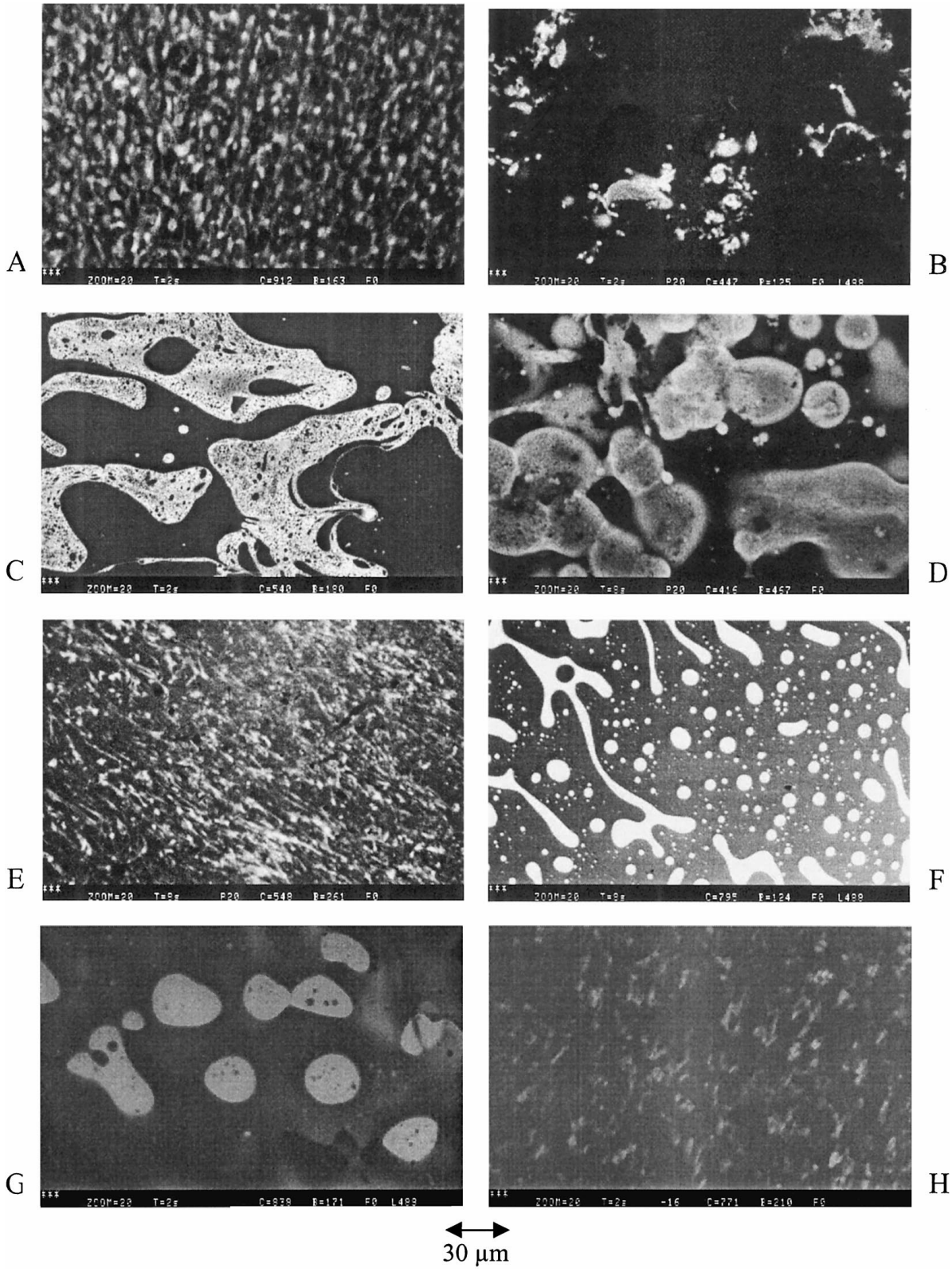

Figure 1 CLSM photographs. (A): blend based on 4% wt. EBA-35 ($\lambda = 543$ nm). (B): blend based on 4% wt. star-shaped SBS_1^* ($\lambda = 488$ nm). (C): blend based on 4% wt. star-shaped SBS_2^* ($\lambda = 514$ nm). (D): blend based on 4% wt. star-shaped SBS_3^* ($\lambda = 543$ nm). (E): blend based on 4% wt. SBS1110 ($\lambda = 543$ nm). (F): blend based on 6% wt. EMA-28 ($\lambda = 543$ nm). (G): blend based on 6% wt. EVA-28 ($\lambda = 543$ nm). (H): blend based on 6% wt. EBA-35 ($\lambda = 488$ and 514 nm).

the asphalt. For example, from the volume fraction of the polymer-rich dispersed phase for the 4 wt. % SB-modified asphalt, the swelling rate can be estimated to 55%. This phenomenon is confirmed by the fact that the two-phase morphology can be evidenced by CLSM even though no fluorescent probe, i.e. Rhodamine®, is added to the polymer before mixing with the asphalt. In fact, the polymer is swollen by aromatics species from the asphalt, the fluorescence of which allow to reveal the polymer domains [31].

For the ethylene copolymers, i.e. EMA and EVA, and for the styrene-butadiene diblock, SB, and star-shaped triblock, SBS, based blends, the CLSM photographs display polymer-rich particles dispersed in a continuous asphalt matrix with similar swelling rates of the polymer as reported in the literature [1, 32]. The interface between the two phases is very sharp and the range of the particles size is respectively between 2 and 25 μm for EMA- and EVA-based blends and between 10 and 50 μm for SB and SBS-based blends. No significant differences are observed in between the two blends based on the styrene-butadiene diblock copolymers which although differ from their molar masses. This phenomenon is in agreement with that reported in the literature [1]. In fact, the molar mass of SB modifiers is not an important parameter for changing the morphology, whereas the particle size is more dependent on the amount of polystyrene [1].

On the opposite, for the poly(ethylene-co-butyl acrylate), EBA, based blends, a co-continuous morphology is evidenced and the interface between the polymer-rich domains and the asphalt-rich matrix is blurred.

3.2. Fracture toughness

The fracture properties measured at -20°C for all the polymer-modified binders are reported in Table IV. The KI_C value of the neat asphalt is equal to 48 ± 9 kPa $\cdot$ m$^{1/2}$ and is in the same order of magnitude as the values reported previously by Hesp for other types of binders [13, 14]. This value is low compared to those of the polymers which are in the order of magnitude of several MPa $\cdot$ m$^{1/2}$. As a consequence, the asphalt displays the fracture behavior of a very brittle material.

TABLE IV KI_C values for different polymer-modified asphalts measured at -20°C

Material	Amount of polymer (% wt.)	KI_C (kPa $\cdot$ m$^{1/2}$)
Neat asphalt	0	48 ± 9
Asphalt/EVA 18	4	39 ± 10
	6	63 ± 15
Asphalt/EVA 28	4	60 ± 13
	6	74 ± 20
Asphalt/EMA 28	4	47 ± 13
	6	67 ± 11
Asphalt/EBA 35	4	64 ± 10
	6	126 ± 20
Star-shaped SBS_1^* (28% m. polystyrene)	4	85 ± 19
Star-shaped SBS_2^* (28% m. polystyrene)	4	107 ± 11
Star-shaped SBS_3^* (18% m. polystyrene)	4	66 ± 15
Diblock SB (12% m. polystyrene)	4	111 ± 16
Styrelf	4	113 ± 21

Table IV shows that SBS* and SB-based blends display higher fracture properties compared to those for mixtures produced with polyethylene-based copolymers. A blend with 4% of SBS or SB exhibits the same KI_C value as the mixture with 6% of EBA. Nevertheless, the compatibility between the polymer and the asphalt and the fracture mechanisms can be different for these two types of blends. The sample prepared with 4% crosslinked SB and the corresponding physical blend (non-crosslinked) display similar properties whereas their morphologies are probably not the same.

ESEM and CSEM were used to examine the fracture surfaces in order to explain the differences in fracture properties observed for the modified-asphalts. The environmental scanning electron micrograph of the neat asphalt shows that the fracture surface is mirror-like (no topographic contrast). As shown earlier from the low value of KIc, the neat binder is a very brittle material.

Three parameters need to be taken in account to explain the fracture mechanisms of the polymer-modified asphalts as for common polymer blends: the type of morphology (dispersed particles vs. co-continuous phases and the distribution of particle size), the volume fraction of the dispersed phase, and the adhesion between the two phases. Numerous papers described in the literature the fracture phenomena occurring as a crack propagates through polymer materials, but apparently no work has been done yet on the fracture mechanisms in polymer-modified asphalts. Nevertheless, the fracture descriptions done for polymer based materials can be of interest for our purpose. The crack front pinning process, initially proposed by Lange [33] and then modified by Evans [34], supposed that the crack can be slowed down or hindered by the presence of particles acting as obstacles. From the creation of additional fracture surface, this phenomenon leads to a higher fracture energy but it supposes that the particles are stiffer than the matrix. In the case where the particles display a ductile behavior and the interfacial adhesion is high, a crack front bridging process is involved. The toughening of heterogeneous materials can be achieved also from the deviation of the crack, from particle to particle (crack deflection mechanism). Finally, a mechanism proposed by Kinloch [35], denoted crack-tip blunting, was proposed to explain the non-stable crack propagation, i.e. the stick-slip mechanism. In the case of polymer-modified asphalts, the stress-strain curve recorded on SEN specimens during bending displays a brittle behavior without a stick-slip propagation of the crack. In addition, the fracture behavior needs to be considered with respect to the difference between the temperature of testing, -20°C, and the T_g's of the components. For the asphalt matrix, the temperature of testing is located at the beginning of the glass transition zone and as a consequence, the continuous phase displays a brittle behavior. This brittleness is also favored by the physical distillation phenomena which

leads to the enrichment of the matrix in asphaltenes acting as rigid nanofillers. As a consequence, whatever the polymeric modifier is, the fracture toughness remains very low (Table IV).

The difference between the temperature of testing and T_g of the polymers depends on the type of polymer (see Tables II and III). In fact, the poly(ethylene-co-vinyl acetate) and poly(ethylene-co-methyl acrylate) are also in a glassy state at the temperature of testing. In fact, their glass transitions are very close to $-20^{\circ}C$, but on the opposite, the poly(ethylene-co-butyl acrylate), EBA, having a T_g of $-45^{\circ}C$ is in the rubbery state. The difference in T_g for EMA and EBA, can explain the slighly higher value of KI_C for the EBA-modified asphalt (Table IV). In fact, the fracture process for the EVA or EMA-based binder involves particle pull-out with no deformation in the asphalt matrix (Figs 2 and 3A). For these blends, the crack bypasses the polymer domains and the fracture occurs at the interface between the two phases. As a consequence, the fracture mechanism is mainly governed by the poor adhesion between the polymer-rich domains and the asphalt matrix.

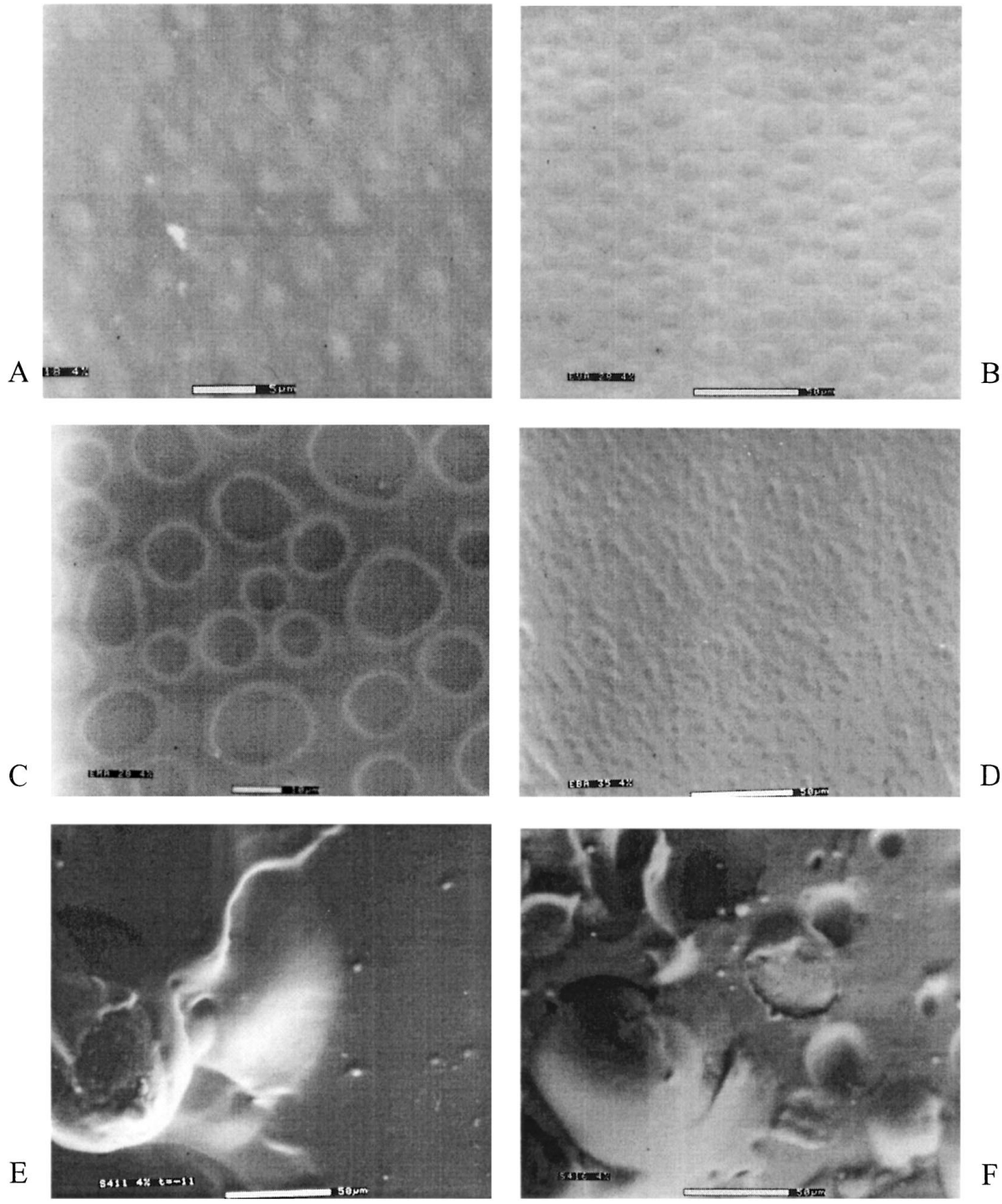

Figure 2 Fracture surfaces (ESEM). (A): blend based on 4% wt. EVA-18. (B): blend based on 4% wt. EVA-28. (C): blend based on 4% wt. EMA-28. (D): blend based on 4% wt. EBA-35. (E): blend based on 4% wt. star-shaped SBS_1^*. (F): blend based on 4% wt. star-shaped SBS_2^*. (G): blend based on 4% wt. star-shaped SBS_3^*. (H): blend based on 4% wt. SB. (I): blend based on 6% wt. EVA-18. (J): blend based on 6% wt. EVA-28. (K): blend based on 6% wt. EMA-28. (L): blend based on 6% wt. EBA-35.

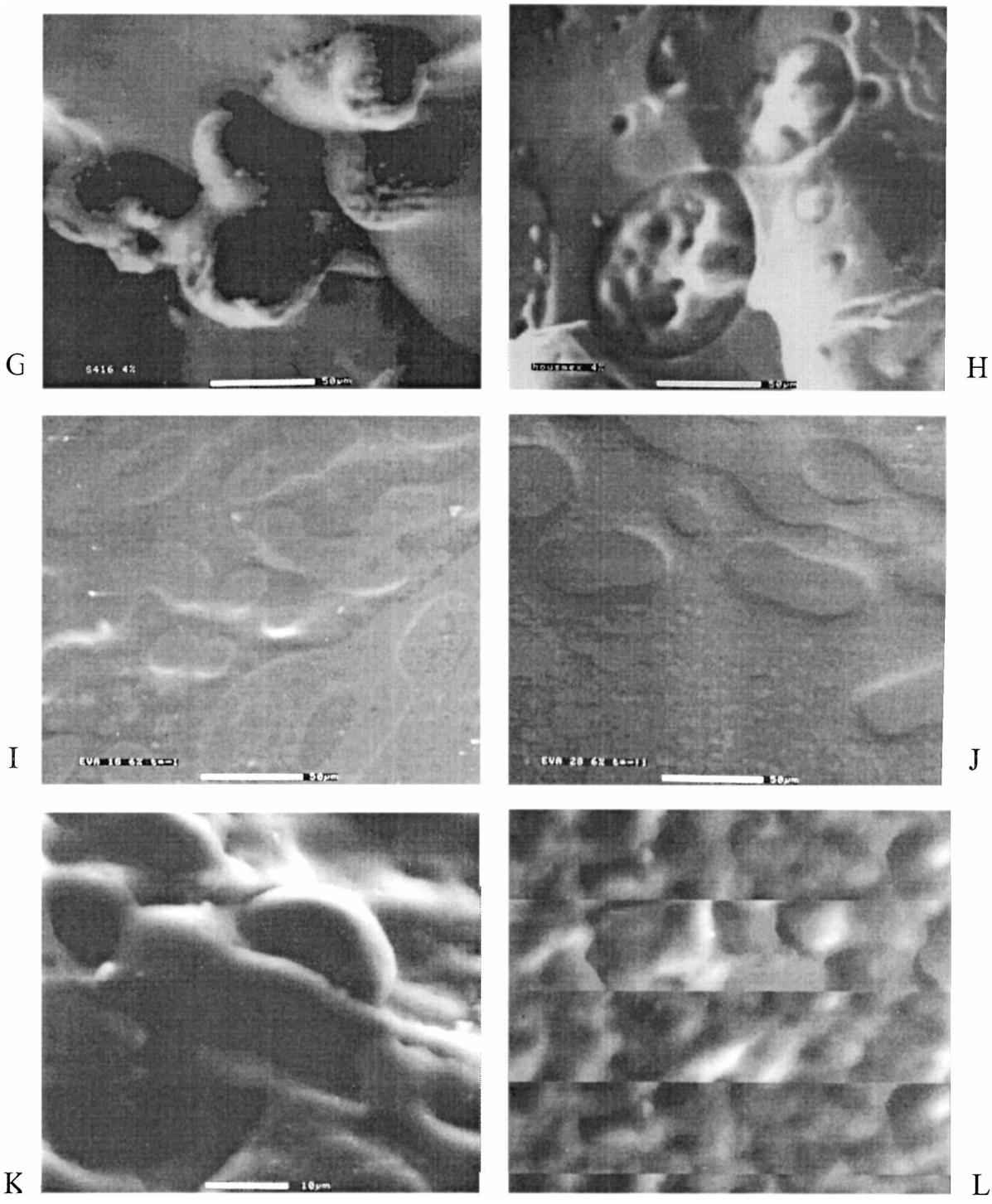

Figure 2 (*Continued.*)

On the opposite, the EBA-based blends display more plastic deformation on the fracture surface, but the interfacial adhesion remains poor (Fig. 2D and L). As a consequence, the fracture toughness remains slighly higher than for the EMA and EVA-blends. In addition, from CLSM, it was demonstrated that the EBA-based blends seem to display a fine co-continuous structure. Thus, the increase of the KI_C value obtained with EBA-modified asphalt compared to EVA- or EMA-modified ones can be associated with the plastic deformation of the polymer phase which is favored by such morphology.

As expected for the polyolefin-based blends, the fracture toughness value is higher for the asphalt modified with 6% polymer (Table IV). The improvement of KI_C can be explained by the increase in volume fraction of the dispersed phase when the polymer content increases from 4 to 6%. These results cannot be compared easily with other data from the literature as only few papers reported KIc values for polymer-modified asphalts. For a 85–100 grade asphalt modified with 3 wt. % of chlorinated polyethylene [15], Hesp reported a value of 154.5 $kPa \cdot m^{1/2}$. Similar values were obtained by Sabbagh and Lesser [13] for LDPE-modified asphalts. The data reported in the literature are in the same order of magnitude than those reported in this work according to the different type of initial asphalts and morphologies. Nevertheless, from the slight differences in the fracture toughnesses of the unstabilized and stabilized

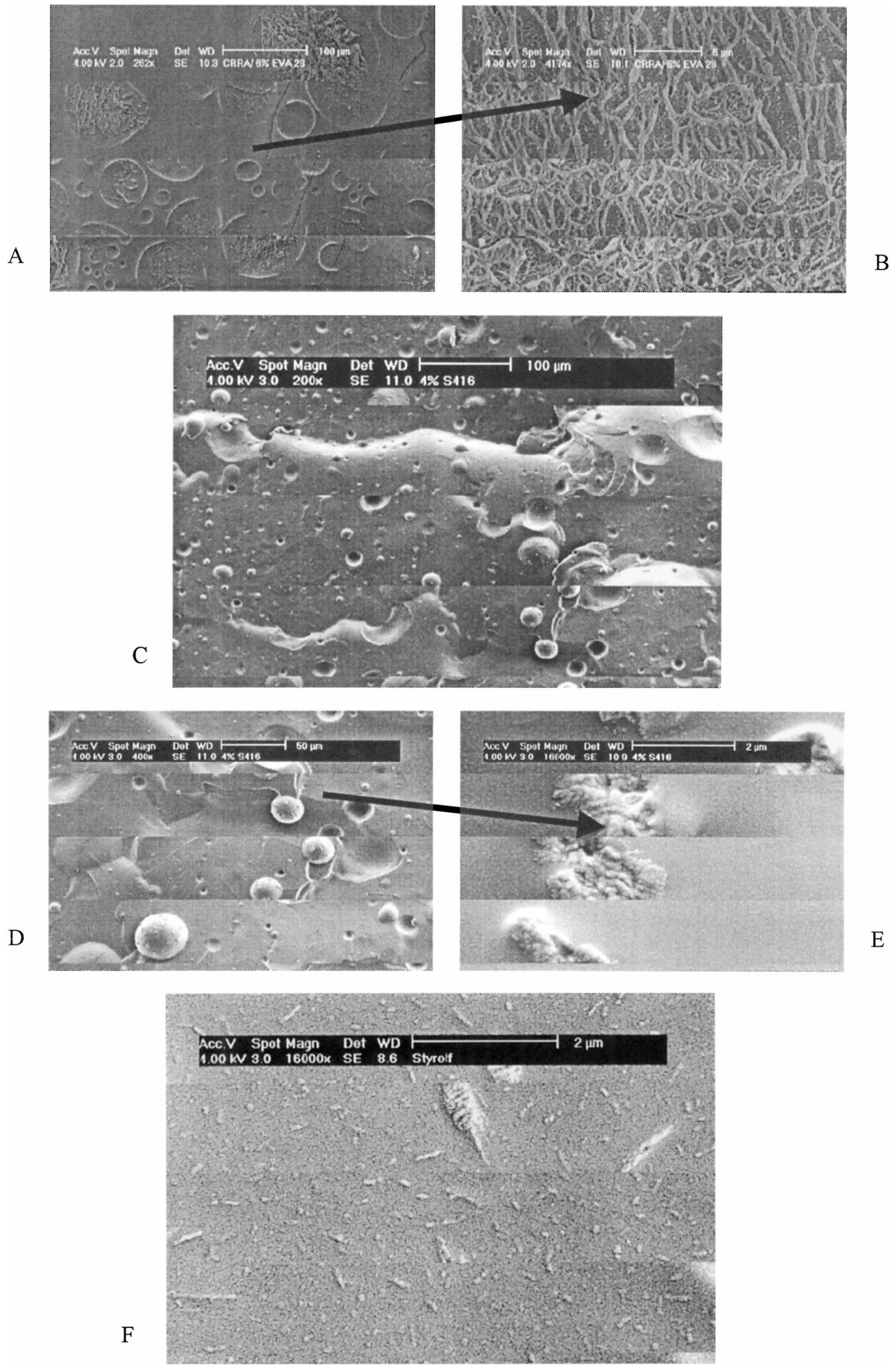

Figure 3 Fracture surfaces (CSEM). (A): blend based on 6% wt. EVA-28. (B): blend based on 6% wt. EVA-28. (C): blend based on 6% wt. SBS^{*}_{2}. (D): blend based on 6% wt. SBS^{*}_{2}. (E): blend based on 6% wt. SBS^{*}_{2}. (F): Styrelf.

emulsion in polyolefin modified asphalts, Sabbagh and Lesser concluded that the toughening mechanisms are not sensitive to the morphology.

For the SBS or SB-based blends, the fracture propagation pattern seems to be different as the fracture surfaces differ from the polyolefin-modified asphalts. For these polymer-asphalt blends, the polymer seems to be stretched as the crack propagates through the polymer domains (Fig. 2C, G, and H). This mechanism, denoted as crack-bridging in polymer blends, requires a good adhesion between the two phases and that the polymer displays the behavior of an elastomer at the temperature of testing. It was previously demonstrated from rheological measurements that the interfacial tension between the polymer-rich dispersed droplets and the continuous asphalt matrix is low [12]. As a consequence, one can assume that the hypothesis of a high interfacial adhesion is verified. In addition, such block copolymers are organized in microdomains and display two glass transitions, corresponding to the PS and PB phases (Table III). In addition, it was demonstrated by transmission electron microscopy that the microdomains organization of such block copolymers remains in the asphalt [31, 36]. Due to the high amount of polybutadiene in the copolymer, having a low glass transition temperature, the polymer-rich phase displays an elastomer-like behavior at the fracture test temperature which is in agreement with the crack-bridging mechanism interpretation. Nevertheless, for the other polymer-asphalt blends, for example with star-shaped SBS_2^* modified asphalt, the fracture surfaces demonstrated that particle pull-out occurs (Fig. 2F) but the fracture toughness remains as for the blends based on the SB diblock copolymers. The higher values of KI_C for these blends can be attributed to the ability of the polymer domains to be plastically deformed before being pulled out (Fig. 3) and to the quite good adhesion at the interface between the polymer phase and the asphalt binder. No topographic contrast is observed on the fracture surface of the binder modified with crosslinked SB due to the morphology which is too fine to be examined using ESEM. On the other hand, the observation of the Styrelf by CSEM reveals that the polymer-rich domains are very small compared to those of the corresponding physical blends (Fig. 3F). The high KI_C value of the chemical blend can be attributed to this fine morphology.

The fracture surfaces are difficult to observe even using the environmental scanning microscopy. In fact, the surface can relaxe after that the fracture propagates and during the time elapsed between the fracture test and the observation in the microscope. By cryo-scanning electron microscopy, the specimens are observed at low temperature. So, the electron beam damage and the modification of the fracture surface are limited. Moreover, the resolution is higher in CSEM compared to ESEM which allows the observation of the Styrelf and the polymer-rich phase more accurately.

T_g's of the asphalt phase and of most of the polymers are in the same range of temperature as the fracture test one. As a consequence, the fracture mechanisms cannot be described as for common polymer blends where one of phase is in the glassy state. Nevertheless, the crack propagation resistance of polymer-modified blends seems related both on the morphology and on the state of the polymer at the temperature of testing, i.e. in the glassy or rubbery state.

4. Conclusions

A mode-I fracture test on SEN specimens has been conducted to measure the fracture properties at low temperature of neat and polymer-modified blends using the linear elastic fracture mechanics (LEFM). The KI_C values need to be discussed as a function of i) the morphology of the blends, i.e. dispersed phase vs. co-continuous structure, volume fraction, distribution of particle size, state of dispersion, and composition of polymer-rich domains and asphalt matrix, and ii) the interfacial adhesion. In fact, as reported previously, the volume fraction of the polymer-rich phase in the blend is higher than the initial amount due to the swelling of the polymer by the aromatic fractions of the asphalt. On the other hand, from the physical distillation of the asphalt when mixed with a polymer, the asphalt matrix is enriched with asphaltenes which can be considered as stiff nanofillers. This study conducted on various asphalt/polymer blends based on different types of polymers, polyolefins or styrene-butadiene block copolymers, demonstrates that the addition of polymer to asphalt increases the fracture toughness at low temperature. However, the improvement is higher with styrene-butadiene copolymers than with polyethylene-based copolymers due to the different toughening mechanisms involved during the crack propagation. Using environmental and cryo-scanning electron microscopy and taking into account the toughening mechanisms described for filled polymers and polymer blends, it was shown that for mixtures with EVA and EMA, the crack propagates at the interface between the polymer-rich phase and the asphalt-rich matrix which displays a brittle behavior whatever the polymer is. This fracture behavior can be explained by the fact that all the components of the blend are at the beginning of their glass transition region at $-20^{\circ}C$, i.e. in the glassy state, and by the poor adhesion between phases. On the opposite, the EBA-based blends display a higher plastic deformation induced in the vicinity of the polymer phase in the asphalt matrix, which can explain the KI_C increase compared to other polyethylene-based copolymers. This effect is related to the lower T_g of poly(ethylene-co-butyl acrylate) which is in a rubbery state at the temperature of testing and by the co-continuous structure observed by CLSM. Such a morphology can contribute also to a higher fracture toughness of the resulting blends. Concerning blends with SB or SBS, the improvement can be explained by a better adhesion between the phases due to a better compatibility between the polymer and the binder which governs the volume fraction and the properties of the polymer phase. In addition, as the microdomains-based structure of the SB or SBS copolymers remain in the blends, the increase of KI_C can be explained by the crack-bridging mechanism reported for polymer

blends. In fact, due to the low T_g of the polybutadiene domains, the polymer-rich domains display an elastomeric behavior at -20°C. Such a behavior is assumed in the crack-bridging mechanism.

This methodology involving the transposition of fracture mechanics from polymer-based materials to asphalt-based ones and original microscopies, confocal laser scanning and environmental and cryo-scanning electron microscopies, is helpful for designing the microstructure of the polymer for an efficient reinforcement of the polymer-modified blends at low temperature. In fact, the compatibility with the asphalt, i.e. the morphology of the polymer-rich phase, and the interfacial adhesion can be defined in order to involve enhancement of the fracture toughness from efficient energy consuming mechanisms.

References

1. B. BRÛLÉ and Y. BRION, *Bull. Liaison LCPC* **145** (1986) 45.
2. G. KRAUS, *Rubber Chem. and Technol.* **55** (1982) 1389.
3. B. BOUTEVIN, Y. PIETRASANTA and J. J. ROBIN, *Progress in Organic Coatings* **17** (1989) 221.
4. G. N. KING, H. W. MUNCY and J. B. PRUD'HOMME, *J. Assoc. Asphalt Paving Technol.* **55** (1986) 519.
5. R. G. MORRISON, R. VAN DER STEL and S. A. M. HESP, *Transportation Research Record* **1515** (1996) 56.
6. G. R. MORRISON and S. A. M. HESP, *J. Materials Sci.* **30** (1995) 2584.
7. Z. Z. LIANG, R. T. WOODHAMS, Z. N. WANG and B. F. HARBINSON, "Use of Waste Materials in Hot-Mix Asphalt," (1993) p. 197.
8. A. H. FAWCETT, T. MCNALLY and G. MCNALLY, in Polymer Preprints, Orlando (1999) p. 216.
9. L. H. LEVANDOWSKI, *Rubber Chemistry and Technology* **67** (1994) 447.
10. V. BRAGA, C. GIAVARINI, V. MUSCARI and M. L. SANTARELLI, *La Rivista dei Combustibili* **47** (1993) 319.
11. S. MACCARRONE, G. HOLLERAN and G. P. GNANASEELAN, in Proceedings 17th ARRB Conference, Part 3, p. 123.
12. D. LESUEUR, J. F. GÉRARD, P. CLAUDY, J. M. LÉTOFFE, D. MARTIN and J. P. PLANCHE, *J. Rheol.* **42**(5) (1998) 1059.
13. J. E. PONNIAH, R. A. CULLEN and S. A. M HESP, in Preprints ACS, Division Fuel Chemistry, Orlando, August 1996, p. 1317.
14. G. R. MORRISON, J. K. LEE and S. A. M. HESP, *J. Appl. Polym. Sci.* **54** (1994) 231.
15. N. K. LEE, G. R. MORRISON and S. A. M. HESP, *AAPT* **64** (1995).
16. A. B. SABBAGH and A. J. LESSER, *Polym. Engng. Sci.* **38**(5) (1998) 707.
17. L. W. CORBETT, *Anal. Chem.* **41** (1968) 576.
18. T. F. YEN, in Preprints of ACS Symposium on Advances in Analysis of Petroleum and its Products, Div. Pet. Chim., New York, 1972.
19. P. CLAUDY, J.M. LÉTOFFÉ and G. N. KING, *Bull. Liaison LCPC* **165** (1990) 85.
20. *Idem., Fuel Sci. Techn. Int.* **9** (1991) 71.
21. D. A. STORM, E. Y. SHEU and R. J. BARRESI, *Proc. Chem. Asphalt* **2** (1991) 813.
22. D. LESUEUR, J. F. GERARD, P. CLAUDY, J. M. LETOFFE, D. MARTIN and J. P. PLANCHE, *J. Rheol.* **40** (1996) 813.
23. M. BROGLY, M. NARDIN and J. SCHULTZ, *J. Appl. Polym. Sci.* **64** (1997) 1903.
24. J. G. WILLIAMS and M. J. CAWOOD, *Polymer Testing* **9** (1990) 15.
25. G. D. DANILATOS, *Microscopy Res. Tech.* **25** (1993) 354.
26. J. I. GOLDSTEIN and H. YAKOWITZ, in "Practical Scanning Electron Microscopy," edited by J. I. Goldstein and H. Yakowitz (Plenum Press, New York, 1976) p. 49.
27. A. W. ROBARDS and A. J. WILSON, in "Procedure in Electron Microscopy," edited by A. W. Robards and A. J. Wilson (John Wiley & Sons, ISBN 0 471 92853 4).
28. H. VERHOOGT, J. VAN DAM, A. POSTHUMA DE BOER, A. DRAAIJER and P. M. HOUPT, *Polymer* **34**(6) (1993) 1325.
29. J. L. THOMASON and A. KNOESTER, *J. Mater. Sci. Lett.* **9** (1990) 258.
30. A. C. RIBES, S. DAMASKINOS, A. E. DIXON, K. A. ELLIST, S. P. DUTTAGUPTA and P. M. FAUCHET, *Progress in Surface Science* **50**(1–4) (1995) 295.
31. M. G. BOULDIN, J. H. COLLINS and A. BERKER, *Rubber Chem. Technol.* **64** (1990) 577.
32. L. LOEBER, A. DURAND and G. MULLER, in Proc. Eurasphalt & Eurobitume Congress, Strasbourg, #5.115, 1996.
33. F. F. LANGE, *Phil. Mag.* **22** (1970) 983.
34. A. G. EVANS, *ibid.* **26** (1972) 1327.
35. A. J. KINLOCH and J. G. WILLIAMS, *J. Mater. Sci.* **15** (1980) 987.
36. A. ADEDEJI, T. GRÜNFELDER, F. S. BATES and C. W. MACOSKO, *Polym. Engng. Sci.* **36** (1996) 1707.

Received 20 September 1999
and accepted 16 May 2000